Journal of Neurotrauma

Journal of Neurotrauma: http://mc.manuscriptcentral.com/neurotrauma

Static and Dynamic Intrinsic Connectivity following Mild Traumatic Brain Injury

Journal:	*Journal of Neurotrauma*
Manuscript ID:	Draft
Manuscript Type:	Regular Manuscript
Date Submitted by the Author:	n/a
Complete List of Authors:	Mayer, Andrew; The Mind Research Network/Lovelace Biomedical and Environmental Research Institute, ; University of New Mexico School of Medicine, Neurology; University of New Mexico, Psychology Ling, Josef; The Mind Research Network/Lovelace Biomedical and Environmental Research Institute, Allen, Elena; The Mind Research Network/Lovelace Biomedical and Environmental Research Institute, Klimaj, Stefan; The Mind Research Network/Lovelace Biomedical and Environmental Research Institute, Yeo, Ron; University of Mexico, Psychology Hanlon, Faith; The Mind Research Network/Lovelace Biomedical and Environmental Research Institute,
Keywords:	ADULT BRAIN INJURY, MRI, TRAUMATIC BRAIN INJURY, NEUROPSYCHOLOGY

Static and Dynamic Intrinsic Connectivity following Mild Traumatic Brain Injury

Andrew R. Mayer, Ph.D.[1,2,3*], Josef M. Ling, B.A.[1], Elena A. Allen, Ph.D.[1], Stefan D. Klimaj, B.S.[1], Ronald A. Yeo, Ph.D.[3], and Faith M. Hanlon, Ph.D.[1]

[1] The Mind Research Network/Lovelace Biomedical and Environmental Research Institute, Albuquerque, New Mexico 87106

[2] Department of Neurology, University of New Mexico School of Medicine, Albuquerque, New Mexico 87131

[3] Department of Psychology, University of New Mexico, Albuquerque, New Mexico 87131

*Corresponding author: Andrew Mayer, Ph.D.

Address for Andrew Mayer, Josef Ling, Elena Allen, Stefan Klimaj, and Faith Hanlon: The Mind Research Network, Pete & Nancy Domenici Hall, 1101 Yale Blvd. NE, Albuquerque, NM 87106; Tel: 505-272- 5028; Fax: 505-272-8002

Address for Ronald Yeo: The Department of Psychology, University of New Mexico Albuquerque, New Mexico 87131; Tel: 505-277-4121; Fax: 505-277-1394

E-mail address: Andrew Mayer - amayer@mrn.org; Josef Ling – jling@mrn.org; Elena Allen – eallen@mrn.org; Stefan Klimaj – sklimaj@mrn.org; Ronald Yeo – ryeo@unm.edu; Faith Hanlon – fhanlon@mrn.org;

Running title: Intrinsic Connectivity in Mild TBI

Key words: mild TBI; resting state networks; ICA; functional; fcMRI

Abstract

Mild traumatic brain injury (mTBI) is the most common neurological disorder and is typically characterized by temporally limited cognitive impairment and emotional symptoms. Previous examinations of intrinsic resting state networks in mTBI have primarily focused on abnormalities in static functional connectivity, and deficits in dynamic functional connectivity have yet to be explored in this population. Resting-state data was collected on 48 semi-acute (mean = 14 days post-injury) mTBI patients and 48 matched healthy controls. A high-dimensional independent component analysis (N = 100) was utilized to parcelate intrinsic connectivity networks (ICN), with a priori hypotheses focusing on the default-mode network (DMN) and sub-cortical structures. Dynamic connectivity was characterized using a sliding window approach over 126 temporal epochs, with standard deviation serving as the primary outcome measure. Finally, distribution-corrected z-scores (DisCo-Z) were calculated to investigate changes in connectivity in a spatially invariant manner on a per-subject basis. Following appropriate correction for multiple comparisons, no significant group differences were evident on measures of static or dynamic connectivity within a priori ICN. Reduced (HC > mTBI patients) static connectivity was observed in the DMN at uncorrected ($p < 0.005$) thresholds. Finally, a trend (p = 0.07) for decreased dynamic connectivity in patients across all ICN was observed during spatially invariant analyses. In the semi-acute phase of recovery, mTBI was not reliably associated with abnormalities in static or dynamic functional connectivity within the DMN or sub-cortical structures.

Introduction

Researchers are increasingly turning to measures of functional connectivity (fcMRI) to examine brain pathology in a variety of neuropsychiatric conditions, including traumatic brain injury (TBI). Functional connectivity studies are based on intrinsic neuronal fluctuations that synchronously occur over spatially distributed networks in humans and non-human primates.[1,2] The majority (60-80%) of the brain's energy resources are expended to maintain homeostasis,[3,4] and intrinsic neuronal activity likely contributes to this heavy energy load. Intrinsic neuronal fluctuations manifest as low-frequency (less than 0.15 Hz) changes in the blood oxygen level dependent (BOLD) response, and are organized into distinct intrinsic connectivity networks (ICN) that closely resemble activity evoked during cognitive tasks.[5-7] Animal[8,9] and human models of chronic, more severe TBI[10] indicate disruption to various ICN following injury. However, despite the large number of individuals who sustain a mild TBI (mTBI) each year,[11] the effects of mTBI on intrinsic activity have only recently been examined. To our knowledge, the nature of dynamic changes in intrinsic activity has yet to be investigated in mTBI.

The majority of fcMRI studies on TBI have focused on connectivity within and between the default-mode network (DMN), which includes both anterior (e.g., the rostral anterior cingulate cortex (rACC)/ventromedial prefrontal cortex) and posterior (e.g., posterior cingulate cortex (PCC), superior temporal/supramarginal gyrus and medial temporal lobes) nodes.[10,12] Reduced fcMRI in the semi-acute stage of mTBI has been observed within the DMN using seed-based analyses, coupled with increased fcMRI between the rACC and ventrolateral prefrontal cortex.[13] Others[14] have reported reduced fcMRI in the posterior hubs (PCC and supramarginal gyrus) of the DMN in conjunction with increased fcMRI within the ventromedial prefrontal cortex using independent component analysis (ICA).

Reduced DMN fcMRI has also been reported in recently concussed athletes, and an increased number of previous mTBI episodes predicted greater abnormality.[15] However, a subsequent study by the same group did not find any significant differences within DMN fcMRI unless a physical stress challenge was presented.[16] Connectivity abnormalities are not only seen within DMN, but also between the DMN and other networks in mTBI. For example, using ICA to examine resting-state fcMRI in blast-induced mTBI patients, Vakhtin et al.[17] found weaker functional connections within six network pairs (DMN-basal ganglia, attention-sensorimotor, frontal-DMN, attention-sensorimotor, attention-frontal, and sensorimotor-sensorimotor). In addition, abnormal fcMRI between the DMN, the task positive network (or the executive network), and the salience network has been found after TBI injury.[10,18]

Disrupted interhemispheric fcMRI in mTBI patients has also been reported in the visual cortex, hippocampus and dorsolateral prefrontal cortex in task-based fcMRI analyses,[19] and similarly, decreased symmetry of fcMRI has been observed based on thalamic seeds.[20] Thalamic seed-based fcMRI has been used during both motor task and resting state, with reports of decreased thalamo-thalamo, thalamo-frontal, and thalamo-temporal fcMRI during resting state and a lack of thalmo-motor fcMRI during the motor task in mTBI.[21] Decreased fcMRI has been observed within the motor-striatal network and increased in the right frontoparietal network in the semi-acute injury phase,[22] with more chronically affected patients exhibiting disrupted fcMRI (both increased and decreased) across 12 different sensory and cognitive networks.[23]

Longitudinal changes in fcMRI have also been described. In mTBI patients with post-concussion syndrome, increased fcMRI in temporal regions was seen at the subacute stage of injury, while decreased fcMRI in frontal regions was seen at the chronic phase.[24] Han et al.[25] used module-based graph theoretic analysis and found abnormal modular organization of cortical

fcMRI in the semi-acute phase of mTBI, yet mixed findings were obtained in follow-up data during the chronic phase. On the basis of these studies and findings from healthy controls (HC), fcMRI appears to be well poised for interrogating fcMRI within all major structures and networks of the brain following mTBI.

To date, all studies examining fcMRI in mTBI have implicitly assumed that the relationships between ICN are static (i.e., temporally stationary). However, individuals are constantly switching between states of high/low attention to the external versus internal environment, between states of high/low arousal, and between states focused on various specialized cognitive activities (e.g., memory versus executive abilities), all of which would likely alter the relationships between ICN during a typical 5-minute resting state scan.[26,27] Recent work in both human[26,28] and non-human[27] primates confirms that fcMRI is not static, and that dynamic changes in fcMRI are not likely to be driven purely by cognitive processes.[27] The temporal stability of fcMRI may reflect the balance of activity between the DMN and the task positive network,[29] suggesting that observed DMN abnormalities in TBI may influence complex system dynamics. Dynamic fcMRI can be measured by examining the variability in fcMRI across a given interval of time (i.e., sliding window) throughout the resting period. Not surprisingly, regions with high global fcMRI profiles such as the lateral posterior parietal cortex, DMN and middle/superior occipital gyri, exhibit the most dynamic fcMRI patterns relative to other ICN.[28]

Our previous studies on evoked hemodynamic activity suggested hypoactivation within the cingulate gyrus and the cerebellum, two deep sub-cortical structures,[30,31] as well as a failure to regulate the DMN.[32] Based on these data and previous results from seed-based analyses,[13] we predicted that mTBI patients would exhibit disruptions in static (decreased fcMRI) and dynamic

(increased variabilitiy) metrics of fcMRI within the DMN and sub-cortical structures. Unlike previous studies, we used a high-dimensional ICA (number of components = 100) to obtain a more fine-grained parcellation of ICN. Finally, given the variability in initial injury conditions during mTBI, we conducted analyses to examine subject-specific abnormalities across all of the ICN.

Materials and Methods

Participants

A total of 51 mTBI participants and 51 HC participated in a series of studies investigating neuronal correlates of semi-acute mTBI. Data from a subset (27 patients) of this cohort has previously been reported using seed-based analyses.[13] Inclusion criteria for the mTBI group were based on the American Congress of Rehabilitation Medicine, including a Glasgow Coma Score of 13-15 (at first contact with medical staff), loss of consciousness (if present) limited to 30 minutes in duration, and post-traumatic amnesia (if present) limited to 24 hours. All mTBI patients were recruited from local Emergency Rooms. mTBI and HC participants were excluded if there was a prior history of neurological disease, major psychiatric disturbance, additional closed head injuries with more than 5 minutes loss of consciousness, additional closed head injuries within the past year, learning disorder, ADHD or a history of substance or alcohol abuse/dependence. Three mTBI patients were identified as outliers (above 3 standard deviations) on at least 2/6 head motion parameters for frame-wise displacement relative to their cohort.[33] These patients and their respective matched controls were subsequently excluded from further analyses, leaving a total of 48 mTBI (23 males; 28.3 +/- 9.5 years old) and 48 HC (23 males; 27.9 +/- 9.6 years old) participants. Informed consent was obtained from all participants according to institutional guidelines at the University of New Mexico.

Patients were evaluated both clinically (mean day post-injury = 13.9 +/- 4.9) and with brain imaging (mean day post-injury = 14.0 +/- 5.3) within 21 days of injury (see Supplementary Table 1). The maximum time between clinical and imaging sessions was 6 days, although it was typically much shorter (mean days between sessions = 1.3 +/- 1.6 for mTBI patients). One mTBI patient and one HC were not able to complete neuropsychological testing due to scheduling difficulties during their first visit. Six of the mTBI subjects were being prescribed various medications for pain related to the accident at the time of their visit.

Clinical Assessment and Imaging Protocol:

The Wechsler Test of Adult Reading (WTAR) and the Test of Memory and Malingering (TOMM) provided estimates of overall pre-morbid intellectual functioning and effort, respectively. Composite indices were calculated for the following cognitive domains: attention (Trails A, Paced Auditory Serial Addition Test, Stroop and WAIS-III digit span), working memory (letter number sequence, arithmetic, and digits backward), processing speed (grooved pegboard and digit symbol coding), executive function (Wisconsin Card Sort, Trails B, and Fluency (FAS)), and memory (California Verbal Learning Test- II). The Neurobehavioral Symptom Inventory (NBSI), a modified version of the Rivermead Questionnaire, the Beck Depression Inventory and State Trait Anxiety Index were also given to measure self-reported post-concussive symptoms and emotional sequelae. Whenever possible, clinical measures were converted to T-scores using published age-specific norms and then averaged to provide an overall composite score for different emotional and cogntive domains (see [30] for additional details).

All images were collected on a 3 Tesla Siemens Trio scanner. Foam padding and paper tape was used to restrict motion within the scanner. High resolution T_1- and T_2-weighted

anatomic images were acquired for all participants (see Supplemental materials). Susceptibility weighted images (SWI) were collected on a subset of 24 mTBI patients to better characterize petechial hemorrhages. A five minute resting state run was completed by each participant using a single-shot, gradient-echo echoplanar pulse sequence [TR = 2000 ms; TE = 29 ms; flip angle = 75°; FOV = 240 mm; matrix size = 64 x 64]. Thirty-three contiguous, axial 4.55-mm thick slices were selected to provide whole-brain coverage (voxel size: 3.75 x 3.75 x 4.55 mm). A total of 152 images were collected, with the first three images eliminated to account for T1 equilibrium effects.

Presentation software (Neurobehavioral Systems) was used for stimulus presentation and synchronization of stimuli with the MRI scanners. Subjects were instructed to passively stare at a foveally presented fixation cross (visual angle = 1.02°) for approximately five minutes and to keep head movement to a minimum.

Image Processing

Functional images were generated and processed using a mixture of freeware and commercial packages. Raw time series images were first despiked (based on the median absolute deviation), temporally interpolated to correct for slice-time acquisition differences, motion-corrected in both two- and three-dimensional space, spatially blurred using a 6 mm Gaussian full-width half-maximum kernel, and then normalized to a 3 mm^3 standard stereotaxic coordinate space (Montreal Neurological Institute) using a non-linear algorithm. Mean frame-wise displacement (FD) was calculated across the 3 displacement parameters and 3 rotational motion parameters derived from the rigid body correction, with rotation converted to millimetres using a 50 mm radius sphere.[34]

A group-level spatial ICA was used to decompose resting state data into independent components using similar parameters from a recent publication.[28] A relatively high model-order was selected for both subject-specific principal components analysis (120 components) as well as group-wise data decomposition (100 components) to provide a more "fine-grained" parcellation of networks. The Infomax ICA algorithm[35] was repeated 20 times in Icasso using random initial conditions,[36] with the group spatial maps estimated as the modes of the component clusters. All group spatial maps were thresholded based on 0.25 of the maximum voxel-wise value to facilitate the automatic selection of components and presentation of data in figures.

Subject-specific spatial maps and component time-courses were estimated using dual (spatial-temporal) regression as implemented in GIFT. Subject-specific time-courses data underwent additional processing to remove potential noise sources.[28] This included 1) detrending linear, quadratic, and cubic trends, 2) multiple regression of the 6 realignment parameters and their temporal derivatives, 3) removal of detected outliers (based on the median absolute deviation), and 4) low-pass filtering with a high-frequency cutoff of 0.15 Hz. Pair-wise correlation coefficients were then computed for all combinations of components, followed by a transformation to z-scores using Fisher's method.

Power spectra were estimated for each participant/component using a multi-taper approach,[37] with the time-bandwidth product set to 3 and the number of tapers set to 5. From each spectrum we calculated the ratio of low (operationally defined as occurring between 0-0.10 Hz band) to high (occurring between the 0.15-0.25 Hz band) frequency power. This ratio should be above approximately 1.5 for ICN based on the temporal properties of the hemodynamic response. A mean power ratio was calculated across all 96 subjects for each component to facilitate automated component selection (see below).

Group components were auto-classified as ICN or artifact (physiological, movement related, or imaging artifacts) using 3 different criteria. Specifically, components were classified as an artifact if the component 1) exhibited peak activations mostly in white matter or ventricles (>50%), 2) exhibited a mean power ratio below 1.5), or 3) a maximum spatial correlation of greater than 0.40 with a component previously classified as artifact in a large cohort of HC.[28] Components were classified as ICN based on a maximum spatial correlation of greater than 0.40 with a component previously classified as an ICN.

Based on these criteria, 41 components were classified as artifact, 52 components as ICN and 7 components as neither ICN nor artifact. All 100 components were then manually reviewed by two trained raters (J.L. and A.M.), with two of the "neither" components reclassified as ICN based on the location of peak activation and the mean power ratio. In addition, one component that was classified as an ICN was manually reclassified as an artifact, leaving a total of 53 ICN. Individual ICN were then assigned (A.M. and J.L.) classified into broad categories of visual, auditory, sensori-motor, sub-cortical, cerebellar, DMN or cognitive control (CCN) networks. Of the 53 ICN, ten were deemed to represent different nodes of the DMN, with six components representing sub-cortical structures (Figure 1A; 16 total *a priori* ICN, i.e. 105 unique pairs).

A sliding window approach was adopted for dynamic fcMRI analyses, wherein correlations were computed from windowed portions of the component time-courses.[28] Specifically, a tapered window was created by convolving a rectangle (width = 24 TRs) with a Gaussian (σ = 3 TRs) function, and slid in steps of 1 TR across all of the TRs. There were a total of 126 different windows in the current analyses (based on 149 initial images and a window width of 24). For each pair of components, the standard deviation across the sliding window correlation time series was then computed as a summary of temporal variability (dynamic

fcMRI). In the current context, larger standard deviations indicate more variable, or less stable, functional connections between two ICN.

Primary analyses were restricted to 16 ICN that were selected to represent the DMN and sub-cortical networks and compared component spatial maps, component spectra, static fcMRI, and dynamic fcMRI between groups. Voxel-wise ANCOVAs using WTAR and mean frame-wise displacement as covariates were utilized to compare spatial maps between mTBI and HC. Group-wise comparisons of subject-specific spatial maps were individually corrected for false positives at $p < 0.05$ based on 10,000 Monte-Carlo simulations. Group comparisons of the power ratio (low/high frequency) across the 16 ICN were performed using a similar ANCOVA model, corrected for multiple comparisons using the Bonferonni method. Group comparisons of pair-wise static and dynamic fcMRI between DMN and sub-cortical ICN (105 pairs each) were conducted with an ANCOVA model and corrected for multiple comparisons using False Discovery Rate (FDR).

Finally, we compared whether mTBI patients exhibited more extreme static or dynamic fcMRI relative to HC in a spatially invariant fashion. First, the mean and standard deviation were calculated for each pair-wise metric from the HC group. The individual pairwise correlations/standard deviations for both HC and mTBI groups were then transformed to signed z-scores using the statistical moments derived from the HC. The z-transformed data for both groups were then corrected for known distributional biases (hereafter referred to as distribution-corrected z-scores; DisCo-Z) resulting from the individual transformations (see Appendix 1; Mayer et al., provisionally accepted). ICN exhibiting extreme values based either on two standard deviations above (DisCo-Z > 2; positive summary measure) or below (DisCo-Z < -2; negative summary measure) the HC mean were coded with a 1 and summed separately across

positive and negative extremes. These single value summary statistics were then transformed by adding one to the count and taking the square root to improve normality. The transformed data were then directly compared across the two groups using WTAR and mean frame-wise displacement as covariates.

Results

Clinical Results

There were no significant group difference ($p > 0.10$) on key demographic variables (see Table 1) including hand preference.[38] Independent samples t-tests indicated that HC achieved higher estimates of premorbid intellectual functioning ($t_{94} = 2.9$, $p = 0.005$) despite educational matching. Therefore, premorbid intelligence was used as a covariate for all analyses. One mTBI patient and two HC performed in the impaired range ($T < 30$) on the TOMM in spite of normal (within 1.5 SD of mean) performance on the remainder of the neuropsychological battery. The data for these participants was subsequently eliminated from the TOMM analysis, with results indicating no group differences ($p > 0.10$).

A MANCOVA comparing the domains of attention, processing speed, working memory, executive functioning and memory with premorbid intelligence as a covariate did not reveal any group differences in cognition ($p > 0.10$) with small to medium effects sizes (Table 1). The multivariate effect from a MANOVA examining self-reported post-concussive symptoms was significant ($F_{3,91} = 12.0$, $p < 0.001$), with univariate effects indicating that mTBI patients in the semi-acute injury phase reported more cognitive ($F_{1,93} = 21.1$, $p < 0.001$), somatic ($F_{1,93} = 30.1$, $p < 0.001$) and emotional ($F_{1,93} = 15.6$, $p < 0.001$) complaints compared to HC.

Anatomical Imaging Results

A total of 8 patients were identified as having complicated mTBI, by virtue of exhibiting trauma-induced pathology on CT (4/36 mTBI patients) or anatomical (T1, T2 or SWI images) MRI (4/48 patients) scans by board-certified neuroradiologists blinded to patient diagnosis. However, there were no gross lesions and findings were spatially variable across the complicated mTBI patients (see Supplemental Table 2).

Motion Parameter Analyses

Two MANOVAs (translations and rotations) were conducted to examine for differences in frame-wise displacement across the two groups. The multivariate effect of group was not significant in either analysis ($p > 0.10$), and none of the univariate analyses approached significance. However, given concerns about the effects of motion on resting state data,[34,39,40] total frame-wise displacement was used as a covariate for all group analyses.

Primary Analyses

All ICN, including spatial maps of the DMN (N=10) and sub-cortical (N=6) regions, are displayed in Figure 1A. Results from ANCOVAs comparing the spatial composition of these ICN indicated no significant differences between mTBI patients and HC following whole-brain correction for false-positives. Similarly, there were no significant differences between mTBI and HC when the low/high frequency power ratios were compared following Bonferroni correction for multiple comparisons ($p < 0.003$). There were no differences in pair-wise static fcMRI within the DMN and sub-cortical ICN following false positive correction using FDR (Figure 1B). Separate static fcMRI matrices are presented for both controls (Figure 1C) and mTBI patients (Figure 1D).

There were no differences in dynamic fcMRI (variability) between HC and mTBI patients following FDR false positive correction within the DMN and sub-cortical ICN (Figure

2B), with pair-wise variability presented separately for both HC (Figure 2C) and mTBI (Figure 2D).

Finally, we also examined subject-specific abnormalities in pair-wise static and dynamic fcMRI between HC and mTBI across all ICN using the DisCo-Z method (i.e., the number of pairs that exceeded a DisCo-Z < -2 or DisCo-Z > 2). There were no differences between patients and controls in terms of static fcMRI ($p > 0.10$; Figure 3A). However, results indicated a statistical trend ($t = -1.81$; $p = 0.07$; Figure 3B) for a decreased number of positive pair-wise extremes for patients relative to controls during dynamic fcMRI analyses.

Exploratory Analyses

Exploratory analyses were performed to examine group differences in static and dynamic fcMRI between all ICN using more liberal statistical criteria ($p < 0.005$ uncorrected for multiple comparisons). Pair-wise comparisons of the 53 ICN resulted in a total of 1378 tests, which would results in approximately seven false positives given an alpha value of 0.005. Consistent with a priori predictions, mTBI patients exhibited decreased static fcMRI between the posterior cingulate cortex and the anterior cingulate/middle frontal gyrus of the DMN (see Table 2). Increased fcMRI for mTBI relative to HC was also observed between mostly sensory ICN (6/8 pairs) including visual, auditory and sensorimotor networks as well as putamen. Increased fcMRI for patients was also observed between the right anterior insula and right inferior frontal gyrus and between bilateral pre-central gyrus and right inferior parietal lobule.

Similar exploratory analyses were conducted on metrics of dynamic fcMRI. Consistent with the DisCo-Z findings, results indicated decreased variability for mTBI patients ($p < 0.005$, uncorrected) relative to HC across 9 different ICN pairs, which predominantly involved either one or two cognitive control ICN (7/9 pairs; Table 3). The remaining two pairs that exhibited

decreased dynamic fcMRI involved the DMN. There was no overlap between ICN showing abnormalities between measures of both static and dynamic fcMRI.

Supplementary Analyses

Two potential differences between current and previous ICA studies on semi-acute mTBI include our post-processing steps to remove motion artifact and our model order (100 components). Supplemental analyses were therefore conducted using minimal subject-specific time-courses post-processing (see Supplemental materials), focusing on the DMN and sub-cortical structures. Results indicated that currently recommended best practices for artifact removal did not have a significant impact on the null results.

The effect of model order (i.e., number of estimated independent components) on static connectivity findings within the DMN was also investigated given previous results in other neuropsychiatric populations.[41] Specifically, ICA analyses were repeated with the exception that two lower-order model decompositions (20 and 30 components) were utilized. However, results indicated no significant differences ($p > 0.10$) within DMN ICN for mTBI patients relative to HC with either the 20 or 30 model order analysis. See Supplemental Figure 1 and Supplemental Table 3 for components and full results.

Discussion

Amongst neuropsychiatric disorders, mTBI offers a unique opportunity for examining transient disruptions in cognitive and emotional functioning and their neuronal correlates in a human model. Similar to previous studies,[42] mTBI patients self-reported increased cognitive, emotional and somatic complaints during the semi-acute injury phase. In contrast, there were no significant cognitive deficits on neuropsychological testing at approximately 14 days post-injury. Previous literature suggests that effect sizes obtained during formal cognitive testing decrease

dramatically as a function of *days* post-injury following a single-episode of mTBI,[43-45] and current testing times may have occurred outside of this relatively short assessment window.

The ICN identified during our high dimensional static ICA are consistent with several other studies,[6,28] demonstrating fcMRI between spatially distinct regions that are arranged into sensory (auditory, visual and sensorimotor) as well as cognitive (DMN and CCN) networks.[5] The exact role of covarying spontaneous fluctuations within ICN has not been fully determined, but they may serve as a record of previous task-dependent usage, may coordinate neuronal activity between regions that are traditionally co-activated, or may represent a dynamic prediction of future use.[46]

Previous studies that examined static fcMRI during the semi-acute stage of mTBI have reported abnormalities within the DMN,[13-15] thalamus[14,20] as well as other ICN.[14,22] In contrast, the current study did not observe any differences in low/high frequency power or static fcMRI in a moderate (N = 48) sample of semi-acutely injured mTBI patients relative to carefully matched controls, which could have been secondary to several factors. First, we utilized currently recommended best practices for removing the effects of head motion on our data, as this has been shown to reduce spurious findings in static fcMRI analyses.[34,39,40] However, data re-analyses *without* the more rigorous motion removal did not ultimately affect our results, suggesting that our efforts at artifact removal did not spuriously remove signal between the two groups.

Second, a high-dimensional ICA decomposition (100 components) was adopted for the current study, which ultimately results in a more fine-grained characterization of individual ICN relative to lower-dimensional solutions[6,28] (Supplemental Figure 1). However, higher dimensional solutions by definition results in a greater number of ICN (i.e., 53 total for current

dataset), which in turn results in more stringent family-wise error correction even with our fairly limited a priori hypotheses (16 DMN and sub-cortical ICN; 105 total pair-wise comparisons). This directly affects the ability to detect group differences (Type II error) while appropriately controlling for false positives (Type I error). Indeed, current findings were suggestive of decreased fcMRI with the anterior and posterior hubs of the DMN (uncorrected $p < 0.005$), consistent with a priori predictions and previous results from a sub-sample of the current data.[13] However, supplemental analyses indicated that these findings were dependent on model-order (i.e., number of independent components estimated), with the lower model-order solutions producing negative results. Therefore, future studies may focus on static fcMRI between these two regions exclusively.

Uncorrected comparisons (uncorrected $p < 0.005$) also indicated increased static fcMRI for mTBI patients between unisensory ICN (6/8 significant pairs). Foremost, these exploratory findings require independent replication due to the unplanned nature of the comparisons and the high likelihood for false positives. With this caveat in mind, neurosensory dysfunction has been reported in both civilian[47] and military TBI[48-51] samples. Resting glucose hypometabolism and/or hypoperfusion has also been reported in auditory and visual sensory cortices using SPECT,[52] PET[53,54] and fMRI[55] in human TBI. Collectively, these findings suggest that future studies should probe the integrity of unisensory cortex following TBI and the relationship between imaging abnormalities and sensory deficits.

To our knowledge, the current study represents the first investigation of how brain trauma affects dynamic fcMRI. Dynamic fcMRI essentially assesses the variability of functional connections between pairs of ICN across a specified temporal window.[26,28] Current results indicated that across both groups, fcMRI was most dynamic (i.e., variable) between and within

the DMN and visual ICN, and most stable for sub-cortical and sensorimotor ICN (superior frontal gyrus and precentral gyrus). However, there were no significant differences in dynamic fcMRI within or between the DMN and sub-cortical ICN across patients and controls. Mild TBI patients also exhibited reduced dynamic connectivity across all ICN at a trend level (DisCo-Z analyses), suggesting that pathologies associated with mTBI may be spatially variable as a result of the different injury mechanisms (Mayer et al., provisionally accepted). Reduced variability was observed for mTBI patients across multiple ICN during uncorrected comparisons (uncorrected $p < 0.005$), most of which occurred in the CCN (7/9 pairs; Figure 2B). As with our unplanned analyses indicating increased static fcMRI in sensory cortex, these results also require independent replication by other groups.

There are several limitations for the current study that should be considered. Foremost, our resting state scan was relatively short (approximately 5 minutes), which may have reduced our ability to detect significant group differences in dynamic fcMRI. Second, patients were scanned approximately two weeks post-injury, which may have limited our ability to detect more rapidly resolving physiological processes. Future studies should consider evaluating patients more immediately post-injury.

In summary, current results indicated evidence of decreased static fcMRI between the anterior and posterior nodes of the DMN during the semi-acute stage of mTBI, but only when data were not fully corrected for false positives ($p < 0.005$). Similarly, there were no significant differences for static or dynamic fcMRI within sub-cortical structures including the thalamus, which previous studies[14,20] have reported as being implicated in semi-acute mTBI. Our uncorrected findings of decreased static fcMRI between anterior and posterior DMN activity,

increased static fcMRI in unisensory cortex and decreased dynamic connectivity in CCN therefore requires replication in independent samples.

Acknowledgements

This work was supported by the National Institutes of Health (grant numbers R21-NS064464-01A1, 3R21NS064464-01A1S1 to A.M). Special thanks to Diana South and Cathy Smith for assistance with data collection.

Author Disclosure Statement

No competing financial interests exist.

References

1. Hutchison, R.M., and Everling, S. (2012). Monkey in the middle: why non-human primates are needed to bridge the gap in resting-state investigations. Front. Neuroanat. 6**,** 29.
2. Raichle, M.E., and Mintun, M.A. (2006). Brain work and brain imaging. Annu. Rev. Neurosci. 29**,** 449-476.
3. Hyder, F., Patel, A.B., Gjedde, A., Rothman, D.L., Behar, K.L., and Shulman, R.G. (2006). Neuronal-glial glucose oxidation and glutamatergic-GABAergic function. J. Cereb. Blood Flow Metab. 26**,** 865-877.
4. Mangia, S., Giove, F., Tkac, I., Logothetis, N.K., Henry, P.G., Olman, C.A., Maraviglia, B., Di, S.F., and Ugurbil, K. (2009). Metabolic and hemodynamic events after changes in neuronal activity: current hypotheses, theoretical predictions and in vivo NMR experimental findings. J. Cereb. Blood Flow Metab. 29**,** 441-463.
5. Smith, S.M., Fox, P.T., Miller, K.L., Glahn, D.C., Fox, P.M., Mackay, C.E., Filippini, N., Watkins, K.E., Toro, R., Laird, A.R., and Beckmann, C.F. (2009). Correspondence of the brain's functional architecture during activation and rest. Proc. Natl. Acad. Sci. U. S. A. 106**,** 13040-13045.
6. Kiviniemi, V., Starck, T., Remes, J., Long, X., Nikkinen, J., Haapea, M., Veijola, J., Moilanen, I., Isohanni, M., Zang, Y.F., and Tervonen, O. (2009). Functional segmentation of the brain cortex using high model order group PICA. Hum. Brain Mapp. 30**,** 3865-3886.
7. Biswal, B.B., Mennes, M., Zuo, X.N., Gohel, S., Kelly, C., Smith, S.M., Beckmann, C.F., Adelstein, J.S., Buckner, R.L., Colcombe, S., Dogonowski, A.M., Ernst, M., Fair, D., Hampson, M., Hoptman, M.J., Hyde, J.S., Kiviniemi, V.J., Kotter, R., Li, S.J., Lin, C.P., Lowe, M.J., Mackay, C., Madden, D.J., Madsen, K.H., Margulies, D.S., Mayberg, H.S.,

McMahon, K., Monk, C.S., Mostofsky, S.H., Nagel, B.J., Pekar, J.J., Peltier, S.J., Petersen, S.E., Riedl, V., Rombouts, S.A., Rypma, B., Schlaggar, B.L., Schmidt, S., Seidler, R.D., Siegle, G.J., Sorg, C., Teng, G.J., Veijola, J., Villringer, A., Walter, M., Wang, L., Weng, X.C., Whitfield-Gabrieli, S., Williamson, P., Windischberger, C., Zang, Y.F., Zhang, H.Y., Castellanos, F.X., and Milham, M.P. (2010). Toward discovery science of human brain function. Proc. Natl. Acad. Sci. U. S. A. 107**,** 4734-4739.

8. Heffernan, M.E., Huang, W., Sicard, K.M., Bratane, B.T., Sikoglu, E.M., Zhang, N., Fisher, M., and King, J.A. (2013). Multi-modal approach for investigating brain and behavior changes in an animal model of traumatic brain injury. J. Neurotrauma 30**,** 1007-1012.
9. Pawela, C.P., Biswal, B.B., Hudetz, A.G., Li, R., Jones, S.R., Cho, Y.R., Matloub, H.S., and Hyde, J.S. (2010). Interhemispheric neuroplasticity following limb deafferentation detected by resting-state functional connectivity magnetic resonance imaging (fcMRI) and functional magnetic resonance imaging (fMRI). Neuroimage 49**,** 2467-2478.
10. Sharp, D.J., Scott, G., and Leech, R. (2014). Network dysfunction after traumatic brain injury. Nat. Rev. Neurol. 10**,** 156-166.
11. Faul, M., Xu, L., Wald, M.M., and Coronado, V.G. (2010). *Traumatic brain injury in the United States: Emergency department visits, hospitalizations, and deaths.* Centers for Disease Control and Prevention, National Center for Injury Prevention and Control: Atlanta (GA).
12. Buckner, R.L., Andrews-Hanna, J., and Schacter, D. (2008). The brain's default network: anatomy, function, and relevance to disease. Ann. N. Y. Acad. Sci. 1124**,** 1-38.
13. Mayer, A.R., Mannell, M.V., Ling, J., Gasparovic, C., and Yeo, R.A. (2011). Functional connectivity in mild traumatic brain injury. Hum. Brain Mapp. 32**,** 1825-1835.

14. Zhou, Y., Milham, M.P., Lui, Y.W., Miles, L., Reaume, J., Sodickson, D.K., Grossman, R.I., and Ge, Y. (2012). Default-mode network disruption in mild traumatic brain injury. Radiology 265**,** 882-892.

15. Johnson, B., Zhang, K., Gay, M., Horovitz, S., Hallett, M., Sebastianelli, W., and Slobounov, S. (2012). Alteration of brain default network in subacute phase of injury in concussed individuals: resting-state fMRI study. Neuroimage 59**,** 511-518.

16. Zhang, K., Johnson, B., Gay, M., Horovitz, S.G., Hallett, M., Sebastianelli, W., and Slobounov, S. (2012). Default mode network in concussed individuals in response to the YMCA physical stress test. J. Neurotrauma 29**,** 756-765.

17. Vakhtin, A.A., Calhoun, V.D., Jung, R.E., Prestopnik, J.L., Taylor, P.A., and Ford, C.C. (2013). Changes in intrinsic functional brain networks following blast-induced mild traumatic brain injury. Brain Inj. 27**,** 1304-1310.

18. Sours, C., Zhuo, J., Janowich, J., Aarabi, B., Shanmuganathan, K., and Gullapalli, R.P. (2013). Default mode network interference in mild traumatic brain injury - a pilot resting state study. Brain Res. 1537**,** 201-215.

19. Slobounov, S.M., Gay, M., Zhang, K., Johnson, B., Pennell, D., Sebastianelli, W., Horovitz, S., and Hallett, M. (2011). Alteration of brain functional network at rest and in response to YMCA physical stress test in concussed athletes: RsFMRI study. Neuroimage 55**,** 1716-1727.

20. Tang, L., Ge, Y., Sodickson, D.K., Miles, L., Zhou, Y., Reaume, J., and Grossman, R.I. (2011). Thalamic resting-state functional networks: disruption in patients with mild traumatic brain injury. Radiology 260**,** 831-840.

21. Zhou, Y., Lui, Y.W., Zuo, X.N., Milham, M.P., Reaume, J., Grossman, R.I., and Ge, Y. (2014). Characterization of thalamo-cortical association using amplitude and connectivity of functional MRI in mild traumatic brain injury. J. Magn. Reson. Imaging 39**,** 1558-1568.

22. Shumskaya, E., Andriessen, T.M., Norris, D.G., and Vos, P.E. (2012). Abnormal whole-brain functional networks in homogeneous acute mild traumatic brain injury. Neurology 79**,** 175-182.

23. Stevens, M.C., Lovejoy, D., Kim, J., Oakes, H., Kureshi, I., and Witt, S.T. (2012). Multiple resting state network functional connectivity abnormalities in mild traumatic brain injury. Brain Imaging Behav. 6**,** 293-318.

24. Messe, A., Caplain, S., Pelegrini-Issac, M., Blancho, S., Levy, R., Aghakhani, N., Montreuil, M., Benali, H., and Lehericy, S. (2013). Specific and evolving resting-state network alterations in post-concussion syndrome following mild traumatic brain injury. PLoS. ONE. 8**,** e65470.

25. Han, K., Mac Donald, C.L., Johnson, A.M., Barnes, Y., Wierzechowski, L., Zonies, D., Oh, J., Flaherty, S., Fang, R., Raichle, M.E., and Brody, D.L. (2014). Disrupted modular organization of resting-state cortical functional connectivity in U.S. military personnel following concussive 'mild' blast-related traumatic brain injury. Neuroimage 84**,** 76-96.

26. Chang, C., and Glover, G.H. (2010). Time-frequency dynamics of resting-state brain connectivity measured with fMRI. Neuroimage 50**,** 81-98.

27. Hutchison, R.M., Womelsdorf, T., Gati, J.S., Everling, S., and Menon, R.S. (2013). Resting-state networks show dynamic functional connectivity in awake humans and anesthetized macaques. Hum. Brain Mapp. 34**,** 2154-2177.

28. Allen, E.A., Damaraju, E., Plis, S.M., Erhardt, E.B., Eichele, T., and Calhoun, V.D. (2014). Tracking whole-brain connectivity dynamics in the resting state. Cereb. Cortex 24**,** 663-676.

29. Hellyer, P.J., Shanahan, M., Scott, G., Wise, R.J., Sharp, D.J., and Leech, R. (2014). The control of global brain dynamics: opposing actions of frontoparietal control and default mode networks on attention. J. Neurosci. 34**,** 451-461.

30. Mayer, A.R., Mannell, M.V., Ling, J., Elgie, R., Gasparovic, C., Phillips, J.P., Doezema, D., and Yeo, R.A. (2009). Auditory orienting and inhibition of return in mild traumatic brain injury: A FMRI study. Hum. Brain Mapp. 30**,** 4152-4166.

31. Yang, Z., Yeo, R., Pena, A., Ling, J., Klimaj, S., Campbell, R., Doezema, D., and Mayer, A. (2012). A fMRI Study of Auditory Orienting and Inhibition of Return in Pediatric Mild Traumatic Brain Injury. J. Neurotrauma 26**,** 2124-2136.

32. Mayer, A.R., Yang, Z., Yeo, R.A., Pena, A., Ling, J.M., Mannell, M.V., Stippler, M., and Mojtahed, K. (2012). A functional MRI study of multimodal selective attention following mild traumatic brain injury. Brain Imaging Behav. 6**,** 343-354.

33. Mayer, A.R., Franco, A.R., Ling, J., and Canive, J.M. (2007). Assessment and quantification of head motion in neuropsychiatric functional imaging research as applied to schizophrenia. J. Int. Neuropsychol. Soc. 13**,** 839-845.

34. Power, J.D., Barnes, K.A., Snyder, A.Z., Schlaggar, B.L., and Petersen, S.E. (2012). Spurious but systematic correlations in functional connectivity MRI networks arise from subject motion. Neuroimage 59**,** 2142-2154.

35. Bell, A.J., and Sejnowski, T.J. (1995). An information-maximization approach to blind separation and blind deconvolution. Neural. Comput. 7**,** 1129-1159.

36. Himberg, J., Hyvarinen, A., and Esposito, F. (2004). Validating the independent components of neuroimaging time series via clustering and visualization. Neuroimage 22**,** 1214-1222.

37. Allen, E.A., Erhardt, E.B., Damaraju, E., Gruner, W., Segall, J.M., Silva, R.F., Havlicek, M., Rachakonda, S., Fries, J., Kalyanam, R., Michael, A.M., Caprihan, A., Turner, J.A., Eichele, T., Adelsheim, S., Bryan, A.D., Bustillo, J., Clark, V.P., Feldstein Ewing, S.W., Filbey, F., Ford, C.C., Hutchison, K., Jung, R.E., Kiehl, K.A., Kodituwakku, P., Komesu, Y.M., Mayer, A.R., Pearlson, G.D., Phillips, J.P., Sadek, J.R., Stevens, M., Teuscher, U., Thoma, R.J., and Calhoun, V.D. (2011). A baseline for the multivariate comparison of resting-state networks. Front. Syst. Neurosci. 5**,** 2.

38. Oldfield, R.C. (1971). The assessment and analysis of handedness: the Edinburgh inventory. Cognitive Neuropsychology 9**,** 97-113.

39. Power, J.D., Mitra, A., Laumann, T.O., Snyder, A.Z., Schlaggar, B.L., and Petersen, S.E. (2014). Methods to detect, characterize, and remove motion artifact in resting state fMRI. Neuroimage 84**,** 320-341.

40. Satterthwaite, T.D., Wolf, D.H., Loughead, J., Ruparel, K., Elliott, M.A., Hakonarson, H., Gur, R.C., and Gur, R.E. (2012). Impact of in-scanner head motion on multiple measures of functional connectivity: relevance for studies of neurodevelopment in youth. Neuroimage 60**,** 623-632.

41. Starck, T., Nikkinen, J., Rahko, J., Remes, J., Hurtig, T., Haapsamo, H., Jussila, K., Kuusikko-Gauffin, S., Mattila, M.L., Jansson-Verkasalo, E., Pauls, D.L., Ebeling, H., Moilanen, I., Tervonen, O., and Kiviniemi, V.J. (2013). Resting state fMRI reveals a default mode dissociation between retrosplenial and medial prefrontal subnetworks in ASD despite motion scrubbing. Front. Hum. Neurosci. 7**,** 802.

42. McCrea, M., Guskiewicz, K.M., Marshall, S.W., Barr, W., Randolph, C., Cantu, R.C., Onate, J.A., Yang, J., and Kelly, J.P. (2003). Acute effects and recovery time following concussion in collegiate football players: the NCAA Concussion Study. JAMA 290**,** 2556-2563.

43. Belanger, H.G., Spiegel, E., and Vanderploeg, R.D. (2010). Neuropsychological performance following a history of multiple self-reported concussions: a meta-analysis. J. Int. Neuropsychol. Soc. 16**,** 262-267.

44. Frencham, K.A., Fox, A.M., and Maybery, M.T. (2005). Neuropsychological studies of mild traumatic brain injury: a meta-analytic review of research since 1995. J. Clin. Exp. Neuropsychol. 27**,** 334-351.

45. Pertab, J.L., James, K.M., and Bigler, E.D. (2009). Limitations of mild traumatic brain injury meta-analyses. Brain Inj. 23**,** 498-508.

46. Fox, M.D., and Raichle, M.E. (2007). Spontaneous fluctuations in brain activity observed with functional magnetic resonance imaging. Nat. Rev. Neurosci. 8**,** 700-711.

47. Sarno, S., Erasmus, L.P., Lipp, B., and Schlaegel, W. (2003). Multisensory integration after traumatic brain injury: a reaction time study between pairings of vision, touch and audition. Brain Inj. 17**,** 413-426.

48. Capo-Aponte, J.E., Urosevich, T.G., Temme, L.A., Tarbett, A.K., and Sanghera, N.K. (2012). Visual dysfunctions and symptoms during the subacute stage of blast-induced mild traumatic brain injury. Mil. Med. 177**,** 804-813.

49. Lew, H.L., Pogoda, T.K., Baker, E., Stolzmann, K.L., Meterko, M., Cifu, D.X., Amara, J., and Hendricks, A.M. (2011). Prevalence of dual sensory impairment and its association with traumatic brain injury and blast exposure in OEF/OIF veterans. J. Head Trauma Rehabil. 26**,** 489-496.

50. Oleksiak, M., Smith, B.M., St Andre, J.R., Caughlan, C.M., and Steiner, M. (2012). Audiological issues and hearing loss among Veterans with mild traumatic brain injury. J. Rehabil. Res. Dev. 49**,** 995-1004.

51. Pogoda, T.K., Hendricks, A.M., Iverson, K.M., Stolzmann, K.L., Krengel, M.H., Baker, E., Meterko, M., and Lew, H.L. (2012). Multisensory impairment reported by veterans with and without mild traumatic brain injury history. J. Rehabil. Res. Dev. 49**,** 971-984.

52. Stamatakis, E.A., Wilson, J.T., Hadley, D.M., and Wyper, D.J. (2002). SPECT imaging in head injury interpreted with statistical parametric mapping. J. Nucl. Med. 43**,** 476-483.

53. Kato, T., Nakayama, N., Yasokawa, Y., Okumura, A., Shinoda, J., and Iwama, T. (2007). Statistical image analysis of cerebral glucose metabolism in patients with cognitive impairment following diffuse traumatic brain injury. J. Neurotrauma 24**,** 919-926.

54. Nakashima, T., Nakayama, N., Miwa, K., Okumura, A., Soeda, A., and Iwama, T. (2007). Focal brain glucose hypometabolism in patients with neuropsychologic deficits after diffuse axonal injury. AJNR Am. J. Neuroradiol. 28**,** 236-242.

55. Kim, J., Whyte, J., Patel, S., Europa, E., Slattery, J., Coslett, H.B., and Detre, J.A. (2012). A perfusion fMRI study of the neural correlates of sustained-attention and working-memory deficits in chronic traumatic brain injury. Neurorehabil. Neural Repair 26**,** 870-880.

Table 1: Neuropsychological and clinical summary measures.

	mTBI	**HC**	
Demographic	Mean (SD)	Mean (SD)	Cohen's d (mTBI – HC)
Age	28.3(9.5)	27.9(9.6)	0.05
Education	13.3(2.3)	13.8(2.3)	-0.21
HQ	82.7(33.5)	83.9(37.1)	-0.03
Neuropsych			
Attention▲	52.2(4.6)	53.2(6.0)	-0.17
Memory▲	51.2(7.9)	51.8(6.9)	-0.09
WM▲	51.8(5.5)	51.7(6.2)	0.02
PS▲	45.3(6.4)	48.0(6.9)	-0.41
EF▲	48.3(5.8)	48.7(5.2)	-0.07
WTAR	50.4(9.0)	55.2(7.7)	-0.58
TOMM	55.0(4.3)	54.4(7.5)	0.10
Self Report			
Emotional	49.3(8.4)	43.3(6.3)	0.81
NBSI-Som	8.0(6.7)	2.2(2.9)	1.12
NBSI-Cog	4.5(3.4)	1.7(2.4)	0.94
Days Post Injury			
Imaging	14.0(5.3)	N/A	N/A
Neuropsych	13.9(4.9)	N/A	N/A

Abbreviations: mTBI = mild traumatic brain injury patients; HC = healthy controls; HQ = handedness quotient; WM = working memory; PS = processing speed; EF = executive function;

WTAR = Wechsler Test of Adult Reading; TOMM = Test of Memory Malingering; NBSI-Cog = Neurobehavioral Symptom Inventory cognitive complaints (Som = somatic complaints); SD = standard deviation; N/A = not applicable.

▲Means, standard deviations and effect sizes for neuropsychological indices reported following correction for WTAR as covariate.

Table 2: Uncorrected ($p < 0.005$) static fcMRI results.

	ICN 1		ICN 2	
***p* value**	**Region**	**Network**	**Region**	**Network**
HC > mTBI				
0.003	PCC	DM	MFG	DM
mTBI > HC				
0.0004	IOG	VS	Cuneus	VS
0.003	MTG	VS	STG	AD
0.004	Cuneus	VS	MTG+STG	AD
0.004	LG	VS	Putamen	SC
0.001	IOG	VS	PreCG	SM
0.001	R IFG	CC	R aInsula	CC
0.004	R IPL	CC	PreCG	SM

Abbreviations: ICN = intrinsic connectivity networks; HC = healthy controls; mTBI = mild traumatic brain injury patients; PCC = posterior cingulate cortex; DM = default mode; MFG = middle fontal gyrus; IOG = inferior occipital gyrus; VS = visual; MTG = medal temporal gyrus; STG = superior temporal gyrus; AD = auditory; LG = lingual gyrus; SC = sub-cortical; PreCG = precentral gyrus; SM = sensorimotor; R IFG = right inferior frontal gyrus; CC = cognitive control; R aInsula = right anterior insula; R IPL = right inferior parietal lobule.

Table 3: Uncorrected ($p < 0.005$) dynamic fcMRI results.

	ICN 1		ICN 2	
***p* value**	**Region**	**Network**	**Region**	**Network**
HC > mTBI				
0.0006	Insula	CC	IFG	CC
0.002	IPL	CC	R IFG	CC
0.004	R IFG	CC	L MFG	CC
0.0002	L MFG	CC	MFG	CC
0.002	IPL	CC	Caudate	SC
0.0004	Insula	CC	Cuneus	VS
0.004	pre-SMA	CC	PreCG	SM
0.0007	MFG	DM	SOG	VS
0.001	Precuneus	DM	PreCG	SM

Abbreviations: ICN = intrinsic connectivity networks; HC = healthy controls; mTBI = mild traumatic brain injury patients; CC = cognitive control; IFG = inferior frontal gyrus; IPL = inferior parietal lobule; R IFG = right inferior frontal gyrus; L MFG = left middle frontal gyrus; MFG = middle fontal gyrus; SC = sub-cortical; VS = visual; pre-SMA = pre-supplementary motor area; PreCG = precentral gyrus; SM = sensorimotor; DM = default mode; SOG = superior occipital gyrus.

Figure Legends

Figure 1: Panel A depicts the 53 intrinsic connectivity networks (ICN) derived across both mild traumatic brain injury (mTBI) patients and healthy controls (HC) following Group-ICA. Individual ICN are clustered into seven over-arching networks: sub-cortical (SC; 6 ICN); default mode (DM; 10 ICN); sensorimotor (SM; 8 ICN); visual (VS; 10 ICN); auditory (AD; 3 ICN); cerebellum (CB; 2 ICN); and cognitive control (CC; 14 ICN). Sagittal (X), coronal (Y) and axial (Z) slice locations are presented according to the Montreal Neurological Institute system. The color-coding for each ICN within each of the seven major networks is presented within Panel B, as well as t-statistics representing the pair-wise comparisons of static fcMRI comparisons across the two groups. Individual ICN labels include: pDMN, posterior default mode network; MeFG, medial frontal gyrus; SFG, superior frontal gyrus; PCC, posterior cingulate cortex; ACC, anterior cingulate cortex; L AG, left angular gyrus; MFG, middle fontal gyrus; L IPL, left inferior parietal lobule; PHG, parahippocampal gyrus; R IPL, right inferior parietal lobule; IPL, inferior parietal lobule; RIFG, right inferior frontal gyrus; IFG, inferior frontal gyrus; MFG, middle frontal gyrus; aInsula, anterior insula; CC, cingulate cortex; L MFG, left middle frontal gyrus; pre-SMA, pre-supplementary motor area; R aInsula, right anterior insula; SPL, superior parietal lobule; SFG, superior frontal gyrus; PreCG, precentral gyrus; PoCG, postcentral gyrus; R PoCG, right postcentral gyrus; SMA, supplementary motor area; PCL, paracentral lobule; L PoCG, left postcentral gyrus; STG, superior temporal gyrus; MTG, medal temporal gyrus; pInsula, posterior insula; FFG, fusiform gyrus; PHG, parahippocampal gyrus; MTG, middle temporal gyrus; LG, lingual gyrus; R MOG, right middle occipital gyrus; L MTG, left middle temporal gyrus; SOG, superior occipital gyrus; IOG, inferior occipital gyrus. A priori hypothesis examined the DM and

SC networks. Panels C and D respectively present the pair-wise pearson correlation values (r) for HC and mTBI patients.

Figure 2: Panels A and B are identical to Figure 1 with the exception that dynamic fcMRI is now contrasted across mild traumatic brain injury (mTBI) patients and healthy controls (HC) in Panel B. Panels C and D presents the standard deviation (SD) of the pair-wise pearson correlation values across the 126 sliding windows for HC and mTBI patients, respectively.

Figure 3: Figure 3 presents box and whisker plots of the DisCo-Z analyses for both negative (NEG) and positive (POS) extreme pair-wise values in static (Panel A) and dynamic (Panel B) connectivity measures. All extreme values were transformed by adding 1 to the count and then taking the square root of extreme measures (1+sqrt). Data from healthy controls (HC) are presented in light gray and mild traumatic brain injury (mTBI) patients' data is presented in dark gray. A trend difference was noted (HC > mTBI) for the positive dynamic fcMRI results.

Figure 1

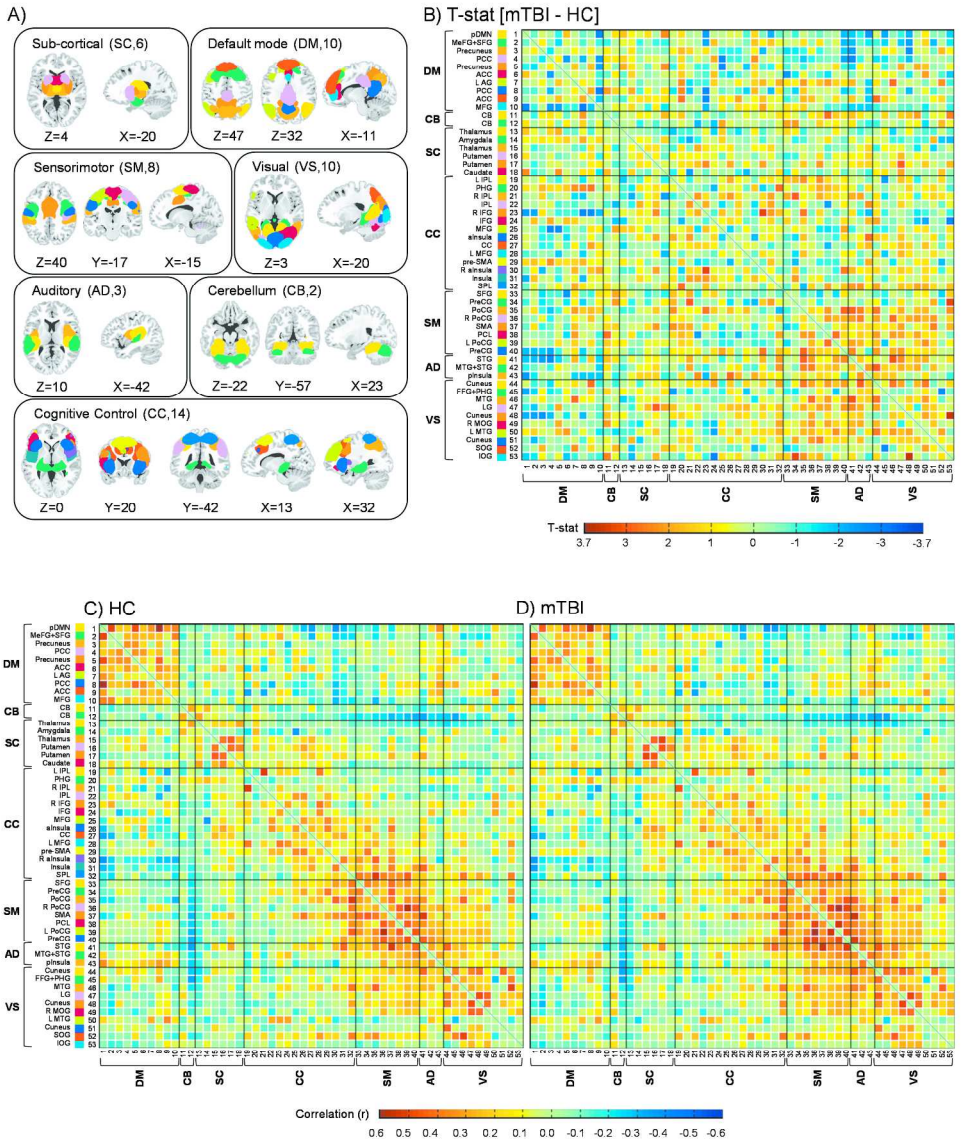

Panel A depicts the 53 intrinsic connectivity networks (ICN) derived across both mild traumatic brain injury (mTBI) patients and healthy controls (HC) following Group-ICA. Individual ICN are clustered into seven over-arching networks: sub-cortical (SC; 6 ICN); default mode (DM; 10 ICN); sensorimotor (SM; 8 ICN); visual (VS; 10 ICN); auditory (AD; 3 ICN); cerebellum (CB; 2 ICN); and cognitive control (CC; 14 ICN). Sagittal (X), coronal (Y) and axial (Z) slice locations are presented according to the Montreal Neurological Institute system. The color-coding for each ICN within each of the seven major networks is presented within Panel B, as well as t-statistics representing the pair-wise comparisons of static fcMRI comparisons across the two groups. Individual ICN labels include: pDMN, posterior default mode network; MeFG, medial frontal gyrus; SFG, superior frontal gyrus; PCC, posterior cingulate cortex; ACC, anterior cingulate cortex; L AG, left angular gyrus; MFG, middle fontal gyrus; L IPL, left inferior parietal lobule; PHG, parahippocampal gyrus; R IPL, right inferior parietal lobule; IPL, inferior parietal lobule; RIFG, right inferior frontal gyrus; IFG, inferior frontal gyrus; MFG, middle frontal gyrus; aInsula, anterior insula; CC, cingulate cortex; L MFG, left middle frontal gyrus; pre-SMA, pre-supplementary motor area; R aInsula, right anterior insula; SPL,

superior parietal lobule; SFG, superior frontal gyrus; PreCG, precentral gyrus; PoCG, postcentral gyrus; R PoCG, right postcentral gyrus; SMA, supplementary motor area; PCL, paracentral lobule; L PoCG, left postcentral gyrus; STG, superior temporal gyrus; MTG, medal temporal gyrus; pInsula, posterior insula; FFG, fusiform gyrus; PHG, parahippocampal gyrus; MTG, middle temporal gyrus; LG, lingual gyrus; R MOG, right middle occipital gyrus; L MTG, left middle temporal gyrus; SOG, superior occipital gyrus; IOG, inferior occipital gyrus. A priori hypothesis examined the DM and SC networks. Panels C and D respectively present the pair-wise pearson correlation values (r) for HC and mTBI patients.

Figure 2

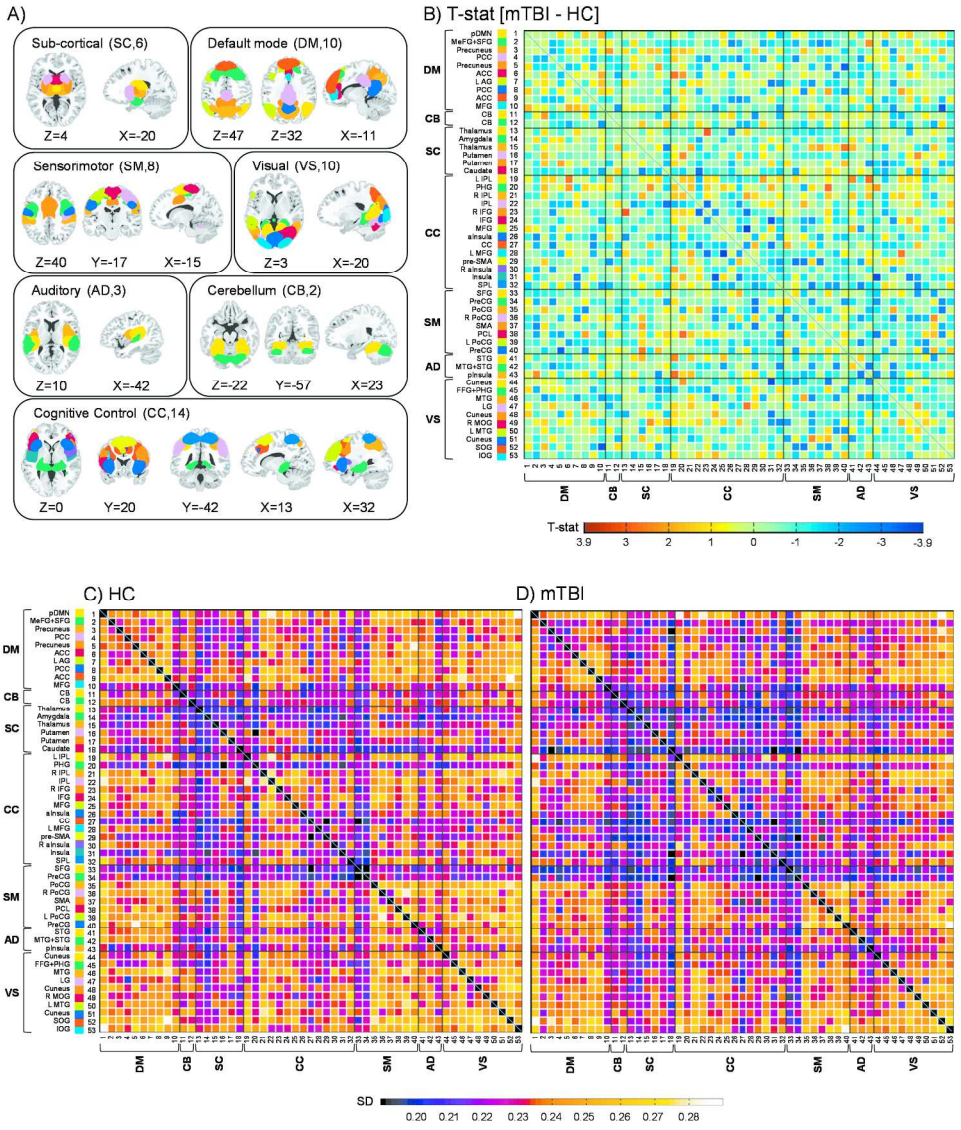

Panels A and B are identical to Figure 1 with the exception that dynamic fcMRI is now contrasted across mild traumatic brain injury (mTBI) patients and healthy controls (HC) in Panel B. Panels C and D presents the standard deviation (SD) of the pair-wise pearson correlation values across the 126 sliding windows for HC and mTBI patients, respectively.

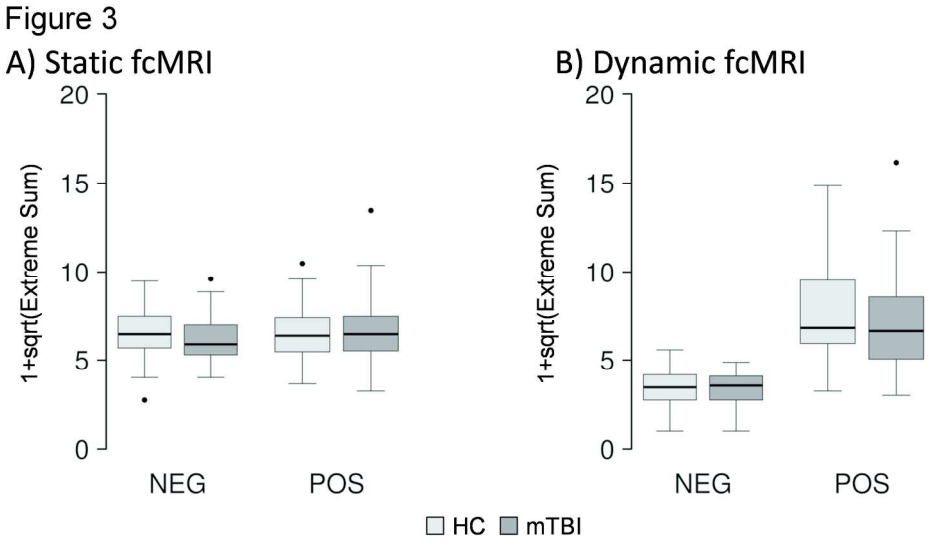

Figure 3 presents box and whisker plots of the DisCo-Z analyses for both negative (NEG) and positive (POS) extreme pair-wise values in static (Panel A) and dynamic (Panel B) connectivity measures. All extreme values were transformed by adding 1 to the count and then taking the square root of extreme measures (1+sqrt). Data from healthy controls (HC) are presented in light gray and mild traumatic brain injury (mTBI) patients' data is presented in dark gray. A trend difference was noted (HC > mTBI) for the positive dynamic fcMRI results.

Supplemental Materials

Imaging Protocol

High resolution T_1-weighted anatomic images were acquired with a 5-echo multi-echo MPRAGE sequence [TE (echo time) = 1.64, 3.5, 5.36, 7.22, 9.08 ms, TR (repetition time) = 2.53 s, TI (inversion time) =1.2s, 7° flip angle, number of excitations (NEX) = 1, slice thickness = 1 mm, FOV (field of view) = 256 mm, resolution = 256 x 256] for all participants. All participants also underwent a T_2-weighted scan with a fast spin echo sequence [TE = 77.0 ms, TR = 1.55 s, flip angle 152°, NEX = 1, slice thickness = 1.5 mm, FOV = 220 mm, matrix = 192x192, voxel size = 1.15x1.15x1.5 mm^3] to examine for structural damage following injury.

Lower-order group-level spatial ICA

Processing and testing methods for lower-order group ICA supplementary analyses were identical to those at the higher model orders with two notable exceptions. First, group-level spatial ICAs were conducted with two separate lower-order model decompositions at 20 and 30 components. Secondly, from the resulting thresholded components, the anterior default-mode network (aDMN), rostral anterior cingulate cortex (rACC), and the posterior default-mode network (pDMN) components were manually identified by expert raters (A.M. and J.L.) at each model order. Pair-wise static fcMRI within these DMN components was tested in an identical fashion to the higher-order group comparisons. Results indicate the effect of group was not significant for either of the lower-order models ($p > 0.10$) (Supplemental Figure 1 and Supplemental Table 3).

Supplemental Table 1: Demographic and injury information for all mTBI patients.

Age	Gender	Injury Mechanism	AAN Rating	Days post-injury		LOC (h:m:s)	PTA (h:m:s)	Number of Previous Injuries*
				MRI	NP			
19	F	Fall	3	18	17	0:03:00	0:00:00	NA
19	F	MVA	3	14	14	0:12:30	24:00:00	NA
20	F	MVA	3	11	11	0:00:00	0:00:03	NA
21	F	MVA	3	14	16	0:05:00	NA	0
21	F	Fall	3	16	15	0:01:20	0:00:00	0
21	F	Fall	3	20	20	0:00:02	0:00:00	1
22	F	Assault	2	18	18	0:00:00	0:03:30	0
22	F	Fall	3	6	7	0:30:00	0:25:00	NA
22	F	MVA	3	11	11	0:02:30	2:10:00	0
22	F	MVA	3	16	16	0:00:00	0:00:05	2
23	F	Assault	1	5	9	0:00:00	0:01:00	NA
23	F	Assault	2	11	11	0:00:00	0:30:00	0
23	F	Assault	3	21	21	0:00:30	0:00:00	0
24	F	Assault	1	7	5	0:00:00	0:00:00	NA
24	F	MVA	3	20	20	0:00:30	1:00:00	NA
25	F	MVA	3	20	20	0:07:30	7:00:00	0
26	F	Fall	3	21	17	0:02:00	0:00:00	0
27	F	Assault	2	8	8	0:00:00	NA	0
27	F	MVA	2	18	13	0:00:00	NA	NA
28	F	Assault	1	11	9	0:00:00	0:05:00	0

28	F	Fall	3	18	20	0:00:30	18:00:00	1
37	F	Fall	3	3	8	0:01:00	0:00:00	0
41	F	Fall	3	17	18	0:01:00	NA	0
48	F	Assault	2	19	19	0:00:00	0:00:00	0
50	F	MVA	3	7	7	0:01:30	4:00:00	NA
18	M	Fall	2	16	20	0:07:30	0:45:00	1
18	M	Assault	2	16	16	0:00:00	0:00:40	0
18	M	Assault	3	17	16	0:00:05	0:00:00	1
19	M	Assault	3	14	15	0:00:03	0:00:00	0
19	M	Fall	3	9	10	0:00:05	0:00:45	1
22	M	MVA	3	20	20	0:00:30	0:00:00	1
23	M	Fall	1	11	7	0:00:00	0:00:00	0
23	M	Fall	3	17	NA	NA	NA	0
24	M	Fall	3	13	13	0:00:03	0:30:00	0
24	M	Fall	3	10	10	0:02:30	0:30:00	0
28	M	MVA	3	15	15	0:00:25	0:00:00	0
30	M	MVA	3	9	9	0:05:00	0:00:00	0
30	M	Assault	3	16	16	0:05:00	24:00:00	0
32	M	Assault	3	3	5	0:01:00	5:00:00	NA
32	M	MVA	3	16	13	0:00:30	0:00:00	0
33	M	Assault	3	20	19	0:00:02	0:03:00	1
33	M	Fall	3	20	19	0:00:15	0:00:00	0
36	M	MVA	3	19	18	0:00:00	2:00:00	1
41	M	Fall	2	18	18	0:00:00	1:00:00	0

45	M	Assault	3	9	9	0:04:00	0:10:00	1
46	M	Fall	2	13	13	0:00:00	0:00:00	0
49	M	Assault	3	7	4	0:02:00	0:00:00	NA
51	M	Fall	2	19	18	0:00:00	24:00:00	0

Note: MVA = motor vehicle accident; AAN = American Academy of Neurology; NP = neuropsychological testing; LOC = loss of consciousness; and PTA = post traumatic amnesia. Duration of LOC and PTA are based on subjective self-report at initial assessment for the study. The assault category also includes injuries sustained from falling objects or during collisions (e.g., sports-related).

*Previous injuries were documented using a modified version of the Rivermead scale, and data collection with this instrument began after the start of the study (not available; NA).

Supplemental Table 2: Radiological findings derived directly from patient chart information.

Findings
CT: "Small amount of subdural blood along the falx and tentorium, with punctate subarachnoid hemorrhage within the vertex. Nasal bone fractures."
CT: "Small amount of subarachnoid hemorrhage layering within the right sylvian fissure without significant mass effect or shift of midline structures"
CT: "Thin right supratentorial subdural hematoma. Right posterior parietal scalp swelling extending to the vertex."
CT: "Left ZMC fracture pattern. Intermediate attenuation fluid within left maxillary sinus, likely hemorrhage."
MRI: "Slight asymmetry of the temporal horn of the right lateral ventricle. Probably, anatomic variant. Subtle T1 hypointensity in the central/left paracentral upper pons. Not well seen on the T2WI's. Question of artifact vs. subtle finding. Consider clinical correlation and possible diagnostic MR."
MRI: "Left maxillary sinus mucous retention cysts. A cluster of small oval fluid signal areas can be found involving the right periatrial/parietal white matter. Largest area measuring about 4 mm. Nonspecific. Could represent dilated virchow robin spaces as other smaller areas of similar signal can be found in the left parietal lobe. Recommend correlation with clinical history and location of injury. REV2: Maxillary sinus mucous retention cysts. Findings most c/w virchow robin spaces mainly in the parietal periventricular white matter. Low signal in the frontal interfalcine area most likely represents dural calcification. Doubtful clinical significance. Recommend clinical correlation nonetheless."
MRI: "Subtle, non-specific white matter lesion in the right centrum semiovale. May be

post-traumatic in nature.”
MRI: “CSF or fluid signal is seen in the left anterior middle cranial fossa, anterior to the temporal lobe. This could represent CSF associated with volume loss of the left temporal lobe. Any history of prior trauma or vascular insult. This CSF signal area could also represent a small arachnoid cyst (2.3 cm x 1.5cm).”

Supplemental Table 3: Results from lower model-order static fcMRI comparisons.

Component Pairs	mTBI	HC		
	Mean(SD)	Mean(SD)	p-value	Cohen's d (mTBI – HC)
Model Order = 20 Components				
rACC and pDMN	0.21(0.23)	0.19(0.19)	0.720	0.08
rACC and aDMN	0.31(0.20)	0.29(0.24)	0.589	0.12
pDMN and aDMN	0.46(0.22)	0.38(0.24)	0.141	0.32
Model Order = 30 Components				
rACC and pDMN	0.17(0.22)	0.14(0.24)	0.490	0.15
rACC and aDMN	0.37(0.25)	0.35(0.24)	0.715	0.08
pDMN and aDMN	0.40(0.20)	0.37(0.22)	0.625	0.11

Note: SD = standard deviation; rACC = rostral anterior cingulate cortex; aDMN = anterior default-mode network; pDMN = posterior default-mode network

Supplemental Figures

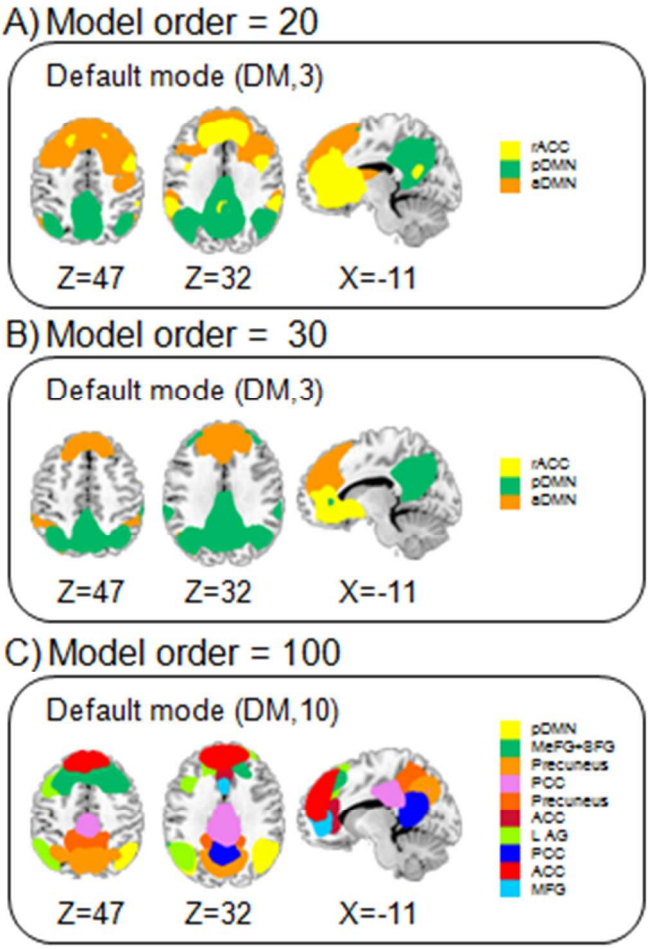

Supplemental Figure 1: Lower model-order ICA results for 20 (Panel A) and 30 (Panel B) components relative to our full model (Panel C and Figures 1 and 2). For the purposes of these analyses we focused on nodes of the default-mode network (DMN), including anterior (aDMN) and posterior aspects (pDMN), as well as the rostral anterior cingulate cortex (rACC).

Appendix

A theoretical consideration of the probability distributions of z-transformed data from the reference (healthy controls) and comparison (patient group) samples is provided. We assume that each observation in a given measurement is standardized by the mean $\bar{X}$ and standard deviation s from the reference group and that the reference and comparison populations have identical multivariate normal (i.e., Gaussian) distributions. For a given voxel, let $Z_R = (X_R - \bar{X})/s$ and $Z_C = (X_C - \bar{X})/s$ be the z−score transforms for random responses X_R and X_C from the reference and comparison populations. The reference group mean $\bar{X}$ and standard deviation s estimate the common population voxel mean μ and standard deviation σ. Regardless of a normality assumption, $\mathrm{Var}(X_C - \bar{X}) = \sigma^2(1 + \frac{1}{N})$ and $\mathrm{Var}(X_R - \bar{X}) = \sigma^2(1 - \frac{1}{N})$, where N is the reference group sample size and Var refers to variance. These variances are different because X_C is statistically independent of $\bar{X}$, whereas X_R and $\bar{X}$ are positively correlated due to $\bar{X}$ being computed from a sample that includes X_R. Consequently, different standardizations of $(X_C - \bar{X})$ and $(X_R - \bar{X})$ are warranted, suggesting that the distributions of Z_C and Z_R are likely different.

Geisser notes that $T_c = \frac{X_C - \bar{X}}{\left\{s\sqrt{1+\frac{1}{N}}\right\}} = Z_c\sqrt{\frac{N}{(N+1)}}$ has a Student's t distribution with $N - 1$ degrees of freedom, written symbolically as $T_C \sim t_{N-1}$ (Geisser, 1993). Cook and Weisberg show that the distribution of the studentized residual $T_R = \frac{X_R - \bar{X}}{\left\{s\sqrt{1-\frac{1}{N}}\right\}} = Z_R\sqrt{\frac{N}{(N-1)}}$ is symmetric about zero with a standard deviation of 1, and that $\frac{T_R^2}{N-1}$ has a Beta distribution with parameters $\frac{1}{2}$ and $\frac{(N-2)}{2}$ (Cook and Weisberg, 1982). As a result, the distributions of Z_C and Z_R differ, which leads to different

probabilities that Z_C and Z_R are more extreme than a common fixed threshold, even when the underlying distributions of X_C and X_R are identical.

Our proposed DisCo-Z correction modifies the z-thresholds so that exceedance probabilities for the two distributions are identical in the null case. We first specify a fixed threshold probability (e.g., $\alpha < 0.05$), and desired upper tail thresholds c_N and r_N that are necessarily a function of N so that

$$\alpha = \Pr(Z_R > r_N) = \Pr(Z_C > c_N) \qquad \text{(Eq. 1)}$$

The arbitrary choice of $\alpha = 0.0228$ corresponds to the probability that a standard normal random variable exceeds a z-score of 2. Using the distributions given above, we demonstrate that the adjusted value for the comparison group is given by

$$c_N = t_{1-\alpha,N-1}\sqrt{1+\frac{1}{N}} \qquad \text{(Eq. 2)}$$

where $t_{1-\alpha,\,N-1}$ is the $100(1-\alpha)$ percentile of the t_{N-1} distribution and N is the reference group sample size.

In contrast, the adjusted threshold for the z-transformed values for the reference group is given by

$$r_N = (N-1)\sqrt{\frac{B(1-2\alpha,0.5,0.5(N-2))}{N}} \qquad \text{(Eq. 3)}$$

where $B(1-2\alpha,\ 0.5,\ 0.5(N-2))$ is the $100(1-2\alpha)$ percentile of a Beta distribution with parameters 0.5 and $0.5(N-2)$. The DisCo-Z thresholds are therefore different for the two samples and dependent on N, with the degree of adjustment decreasing as a function of increasing N.